



Precise and Ultrafast Molecular Sieving Through Graphene Oxide Membranes

R. K. Joshi *et al.*

Science **343**, 752 (2014);

DOI: 10.1126/science.1245711

This copy is for your personal, non-commercial use only.

If you wish to distribute this article to others, you can order high-quality copies for your colleagues, clients, or customers by [clicking here](#).

Permission to republish or repurpose articles or portions of articles can be obtained by following the guidelines [here](#).

The following resources related to this article are available online at www.sciencemag.org (this information is current as of February 16, 2014):

Updated information and services, including high-resolution figures, can be found in the online version of this article at:

<http://www.sciencemag.org/content/343/6172/752.full.html>

Supporting Online Material can be found at:

<http://www.sciencemag.org/content/suppl/2014/02/12/343.6172.752.DC1.html>

A list of selected additional articles on the Science Web sites **related to this article** can be found at:

<http://www.sciencemag.org/content/343/6172/752.full.html#related>

This article **cites 47 articles**, 7 of which can be accessed free:

<http://www.sciencemag.org/content/343/6172/752.full.html#ref-list-1>

This article has been **cited by** 1 articles hosted by HighWire Press; see:

<http://www.sciencemag.org/content/343/6172/752.full.html#related-urls>

This article appears in the following **subject collections**:

Materials Science

http://www.sciencemag.org/cgi/collection/mat_sci

Precise and Ultrafast Molecular Sieving Through Graphene Oxide Membranes

R. K. Joshi,¹ P. Carbone,² F. C. Wang,³ V. G. Kravets,¹ Y. Su,¹ I. V. Grigorieva,¹ H. A. Wu,³ A. K. Geim,^{1*} R. R. Nair^{1*}

Graphene-based materials can have well-defined nanometer pores and can exhibit low frictional water flow inside them, making their properties of interest for filtration and separation. We investigate permeation through micrometer-thick laminates prepared by means of vacuum filtration of graphene oxide suspensions. The laminates are vacuum-tight in the dry state but, if immersed in water, act as molecular sieves, blocking all solutes with hydrated radii larger than 4.5 angstroms. Smaller ions permeate through the membranes at rates thousands of times faster than what is expected for simple diffusion. We believe that this behavior is caused by a network of nanocapillaries that open up in the hydrated state and accept only species that fit in. The anomalously fast permeation is attributed to a capillary-like high pressure acting on ions inside graphene capillaries.

Porous materials with a narrow distribution of pore sizes, especially in the angstrom range (1–5), are of interest for use in separation technologies (5–7). The observation of fast permeation of water through carbon nanotubes (8–10) and, more recently, through graphene-oxide (GO) laminates (11) has led to many proposals to use these materials for nanofiltration and desalination (8–19). GO laminates are particularly attractive because they are easy to fabricate and mechanically robust and should be amenable to industrial-scale production (20, 21). They are made of impermeable functionalized graphene sheets that have a typical size of $L \approx 1 \mu\text{m}$ and the interlayer separation, d , sufficient to accommodate a mobile layer of water (11–25). Nanometer-thick GO films have recently been tried for pressure-driven filtration, revealing promising characteristics (15–18). However, the results varied widely for different fabrication methods, and some observations relevant to the present report (permeation of large molecules) are inconsistent with the known structure of GO laminates (20, 21). This suggests the presence of cracks or pin holes in those GO thin films, which obscured their intrinsic properties (25).

We studied micrometer-thick GO membranes prepared from GO suspensions using vacuum filtration as described in (25). The resulting membranes were checked for their continuity by using a helium leak detector before and after filtration experiments, which demonstrated that the mem-

branes were vacuum-tight in the dry state (11). Schematics of our permeation experiments are shown in Fig. 1. The feed and permeate compartments were initially filled to the same height with different liquids, including water, glycerol, toluene, ethanol, benzene, and dimethyl sulfoxide (DMSO). No permeation could be detected over a period of many weeks by monitoring liquid levels and using chemical analysis (25). If both compartments were filled with water solutions,

permeation through the same vacuum-tight membrane could be readily observed as rapid changes in liquid levels (several millimeters per day). For example, a level of a 1 M sucrose solution in the feed compartment rose, whereas it fell in the permeate compartment filled with deionized water. For a membrane with a thickness h of $1 \mu\text{m}$, we found water flow rates of $\approx 0.2 \text{ L m}^{-2} \text{ h}^{-1}$, and the speed increased with increasing the molar concentration C . Because a 1 M sucrose solution corresponds to an osmotic pressure of $\approx 25 \text{ bar}$ at room temperature (the van't Hoff factor is 1 in this case), the flow rates agree with the evaporation rates of $\approx 10 \text{ L m}^{-2} \text{ h}^{-1}$ reported for similar membranes in (11), in which case, the permeation was driven by a capillary pressure of the order of 1000 bar. The hydrostatic pressures in our experiments never exceeded 10^{-2} bar and, therefore, could be neglected.

We next investigated the possibility that dissolved ions and molecules could diffuse through the capillaries simultaneously with water. We filled the feed compartment with various solutions to determine whether any of the solutes permeated into the deionized water on the other side of the GO membrane (Fig. 1B). As a quick test, ion transport can be probed by monitoring electrical conductivity of the permeate compartment (fig. S1). We found that for some salts (for example, NaCl), the conductivity increased with time, but for others {for example, $\text{K}_3[\text{Fe}(\text{CN})_6]$ }, it did not change over many days of measurements.

Depending on the solute, we used ion chromatography, inductively coupled plasma optical

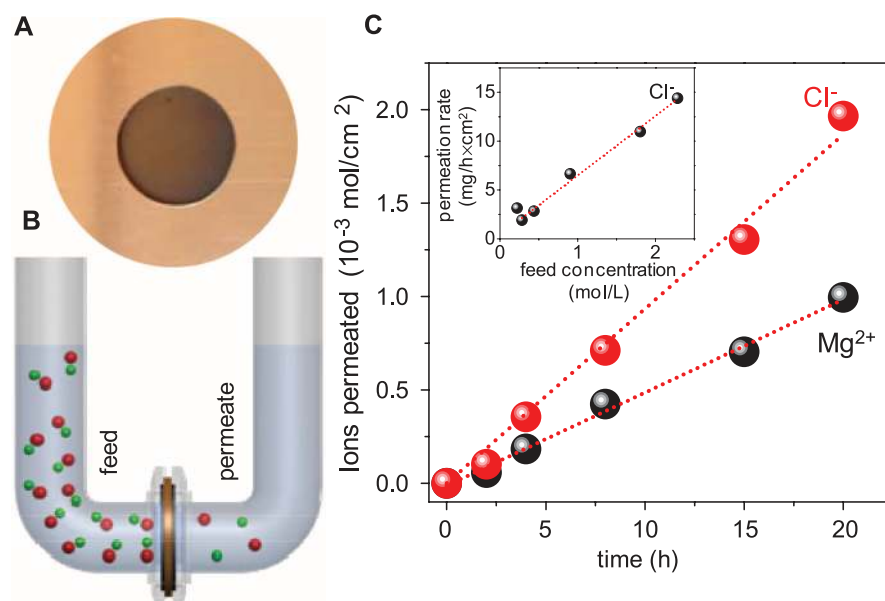


Fig. 1. Ion permeation through GO laminates. (A) Photograph of a GO membrane covering a 1-cm opening in a copper foil. (B) Schematic of the experimental setup. A U-shaped tube 2.5 cm in diameter is divided by the GO membrane into two compartments referred to as feed and permeate. Each is filled to a typical level of $\sim 20 \text{ cm}$. Magnetic stirring is used so as to ensure no concentration gradients. (C) Permeation through a $5\text{-}\mu\text{m}$ -thick GO membrane from the feed compartment with a 0.2 M solution of MgCl_2 . (Inset) Permeation rates as a function of C in the feed solution. Within our experimental accuracy (variations by a factor of $<40\%$ for membranes prepared from different GO suspensions), chloride rates were found the same for MgCl_2 , KCl , and CuCl_2 . Dotted lines are linear fits.

¹School of Physics and Astronomy, University of Manchester, Manchester M13 9PL, UK. ²School of Chemical Engineering and Analytical Science, University of Manchester, Manchester M13 9PL, UK. ³Chinese Academy of Sciences Key Laboratory of Mechanical Behavior and Design of Materials, Department of Modern Mechanics, University of Science and Technology of China, Hefei, Anhui 230027, China.

*Corresponding author. E-mail: rahu.l.raveendran-nair@manchester.ac.uk (R.R.N.); geim@man.ac.uk (A.K.G.)

emission spectrometry, total organic carbon analysis, and optical absorption spectroscopy (25) to measure permeation rates for a range of molecules and ions (table S1). An example of our measurements for MgCl_2 is shown in Fig. 1C, using ion chromatography and inductively coupled plasma optical emission spectrometry for Mg^{2+} and Cl^- , respectively. Concentrations of Mg^{2+} and Cl^- in the permeate compartment increased linearly with time, as expected. Slopes of such curves yield permeation rates. The observed rates depend linearly on concentration in the feed compartment (Fig. 1C, inset). Cations and anions move

through membranes in stoichiometric amounts so that charge neutrality within each of the compartment is preserved. For example, in Fig. 1C permeation of one Mg^{2+} ion is accompanied by two Cl^- ions, and there is no electric field buildup across the membrane.

Our results obtained for different ionic and molecular solutions are summarized in Fig. 2. The small species permeate with approximately the same speed, whereas large ions and organic molecules exhibit no detectable permeation. The effective volume occupied by an ion in water is characterized by its hydrated radius. If plotted

as a function of this parameter, our data are well described by a single-valued function with a sharp cutoff at ≈ 4.5 Å (Fig. 2). Species larger than this are sieved out. This behavior corresponds to a physical size of the mesh of ≈ 9 Å. Also, permeation rates do not exhibit any notable dependence on ion charge (Fig. 2) (12, 13, 23, 26) because triply charged ions such as AsO_4^{3-} permeate with approximately the same rate as singly charged Na^+ or Cl^- . Last, to prove the essential role of water for ion permeation through GO laminates, we dissolved KCl and CuSO_4 in DMSO, the polar nature of which allows solubility of these salts. No permeation was detected, confirming the special affinity of GO laminates to water.

To explain the observed sieving properties, we use the model previously suggested to account for unimpeded evaporation of water through GO membranes (11). Individual GO crystallites have two types of regions: functionalized (oxidized) and pristine (21, 27, 28). The former regions act as spacers that keep adjacent crystallites apart and also prevent them from being dissolved. In a hydrated state, the spacers help water to intercalate between GO sheets, whereas pristine regions provide a network of capillaries that allow nearly frictionless flow of a layer of correlated water, similar to the case of water transport through carbon nanotubes (8–10). The earlier experiments using GO laminates in air (typical $d \approx 9 \pm 1$ Å) were explained by assuming one monolayer of moving water. For GO laminates soaked in water, d increases to $\approx 13 \pm 1$ Å (fig. S2), which allows two or three water layers (19, 22, 23, 29). Taking into account the effective thickness of graphene of 3.4 Å (interlayer distance in graphite), this yields a pore size of ≈ 9 to 10 Å, which is in agreement with the mesh size found experimentally.

To support our model, we have used molecular dynamics (MD) simulations. The setup is shown in Fig. 3A, in which a graphene capillary separates feed and permeate reservoirs, and its width is varied between 7 and 13 Å to account for the possibility of one, two, or three layers of water (25). We find that the narrowest

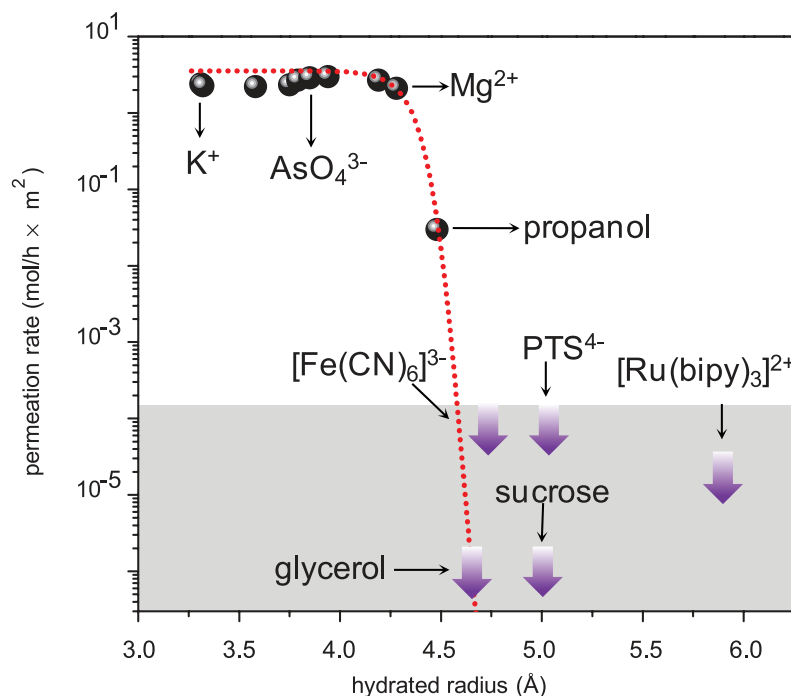
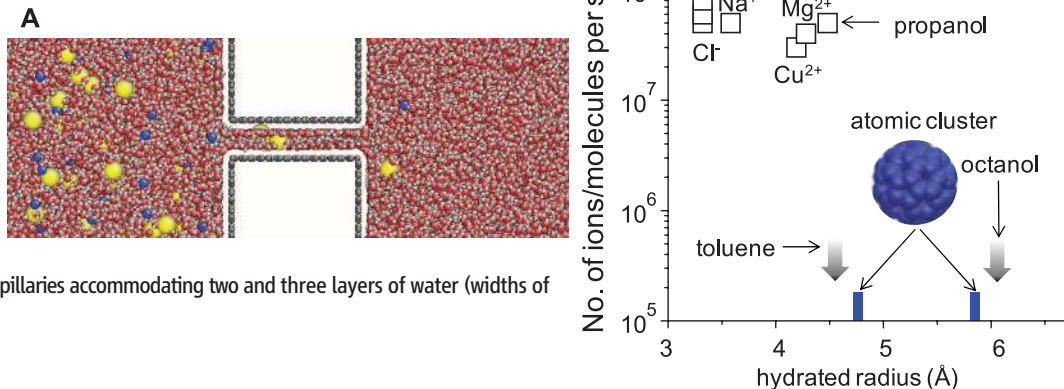


Fig. 2. Sieving through the atomic-scale mesh. The shown permeation rates are normalized per 1 M feed solution and measured by using 5- μm -thick membranes. Some of the tested chemicals are named here; the others can be found in table S1 (25). No permeation could be detected for the solutes shown within the gray area during measurements lasting for at least 10 days. The thick arrows indicate our detection limit, which depends on a solute. Several other large molecules—including benzoic acid, DMSO, and toluene—were also tested and exhibited no detectable permeation. The dashed curve is a guide to the eye, showing an exponentially sharp cutoff at 4.5 Å, with a width of ≈ 0.1 Å.

Fig. 3. Simulations of molecular sieving. (A) Snapshot of NaCl diffusion through a 9 Å graphene slit allowing two layers of water.

Na^+ and Cl^- ions are in yellow and blue, respectively. (B) Permeation rates for NaCl, CuCl_2 , MgCl_2 , propanol, toluene, and octanol for such capillaries. For octanol poorly dissolved in water, the hydrated radius is not known, and we use its molecular radius. Blue marks indicate permeation cutoff for an atomic cluster (inset) for graphene capillaries accommodating two and three layers of water (widths of 9 and 13 Å, respectively).



capillaries become filled with a monolayer of water as described previously (11) and do not allow even such small ions as Na^+ and Cl^- inside. However, for two and three layers expected in the fully hydrated state (25) ions enter the capillaries and diffuse into the permeate reservoir. Their diffusion rates are found to be approximately the same for all small ions and show little dependence on ionic charge (Fig. 3B). Larger species (toluene and octanol) cannot permeate even through capillaries containing three layers of water (fig. S3). We have also modeled large solutes as atomic clusters of different size (25) and found that the capillaries accommodating two and three layers of water rejects clusters with the radius larger than ≈ 4.7 and 5.8 Å, respectively. This may indicate that the ion permeation through GO laminates is limited by regions containing two layers of water. The experimental and theory results in Figs. 2 and 3B show good agreement.

Following (11), we estimate that for our laminates with $h \approx 5$ μm and $L \approx 1$ μm, the effective length of graphene capillaries is $L \times h/d \approx 5$ mm and that they occupy $d/L \approx 0.1\%$ of the surface area. This estimate is supported by measuring the volume of absorbed water, which is found to match the model predictions (25). For a typical diffusion coefficient of ions in water ($\approx 10^{-5}$ cm² s⁻¹), the expected diffusion rate for a 1 M solution through GO membrane is $\approx 10^{-3}$ mol h⁻¹ m⁻² (25)—that is, several thousands of times smaller than the rates observed experimentally (Fig. 1C). Such fast transport cannot be explained by the confinement, which increases the diffusion coefficient by only a factor of 3/2, reflecting the change from bulk to two-dimensional water. Moreover, functionalized regions [modeled as graphene with randomly attached epoxy and hydroxyl groups (20, 21)] do not enhance diffusion but rather suppress it (25, 29) as expected because of the broken translational symmetry.

To understand the ultrafast ion permeation, we recall that graphite-oxide powders exhibit extremely high absorption efficiency with respect to many salts (30). Despite being densely stacked, our GO laminates are found to retain this property for salts with small hydrated radii [(25), section 6]. Our experiments show that permeating salts are absorbed in amounts reaching as much as 25% of the membrane's initial weight (fig. S2). The large intake implies highly concentrated solutions inside graphene capillaries (close to the saturation). Our MD simulations confirm that small ions prefer to reside inside capillaries (fig. S4). The affinity of salts to graphene capillaries indicates an energy gain with respect to the bulk water, and this translates into a capillary-like pressure that acts on ions within a water medium (25). Therefore, there is a large capillary force, sucking small ions inside GO laminates and facilitating their permeation. Our MD simulations provide an estimate for this ionic pressure as >50 bars (25).

The reported GO membranes exhibit extraordinary separation properties, and their full understanding will require further work both experimental and theoretical. With the ultrafast ion transport and atomic-scale pores, GO membranes already present an interesting material to consider for separation and filtration technologies, particularly those that target extraction of valuable solutes from complex mixtures. By avoiding the swelling of GO laminates in water (by using mechanical constraints or chemical binding), it may be possible to reduce the mesh size down to ~ 6 Å; in which case, one monolayer of water would still go through, but even the smallest salts would be rejected.

References and Notes

1. K. B. Jirage, J. C. Hulteen, C. R. Martin, *Science* **278**, 655–658 (1997).
2. N. B. McKeown, P. M. Budd, *Chem. Soc. Rev.* **35**, 675–683 (2006).
3. D. L. Gin, R. D. Noble, *Science* **332**, 674–676 (2011).
4. D. Cohen-Tanugi, J. C. Grossman, *Nano Lett.* **12**, 3602–3608 (2012).
5. S. P. Koenig, L. Wang, J. Pellegrino, J. S. Bunch, *Nat. Nanotechnol.* **7**, 728–732 (2012).
6. M. Ulbricht, *Polymer (Guildf.)* **47**, 2217–2262 (2006).
7. M. Elimelech, W. A. Phillip, *Science* **333**, 712–717 (2011).
8. J. K. Holt et al., *Science* **312**, 1034–1037 (2006).
9. M. Majumder, N. Chopra, R. Andrews, B. J. Hinds, *Nature* **438**, 44 (2005).
10. G. Hummer, J. C. Rasaiah, J. P. Noworyta, *Nature* **414**, 188–190 (2001).
11. R. R. Nair, H. A. Wu, P. N. Jayaram, I. V. Grigorieva, A. K. Geim, *Science* **335**, 442–444 (2012).
12. M. Majumder, N. Chopra, B. J. Hinds, *J. Am. Chem. Soc.* **127**, 9062–9070 (2005).
13. F. Fornasiero et al., *Proc. Natl. Acad. Sci. U.S.A.* **105**, 17250–17255 (2008).
14. L. Qiu et al., *Chem. Commun. (Camb.)* **47**, 5810–5812 (2011).
15. P. Sun et al., *ACS Nano* **7**, 428–437 (2013).
16. Y. Han, Z. Xu, C. Gao, *Adv. Funct. Mater.* **23**, 3693–3700 (2013).
17. M. Hu, B. Mi, *Environ. Sci. Technol.* **47**, 3715–3723 (2013).
18. H. Huang et al., *Chem. Commun. (Camb.)* **49**, 5963–5965 (2013).
19. K. Raidongia, J. Huang, *J. Am. Chem. Soc.* **134**, 16528–16531 (2012).
20. D. A. Dikin et al., *Nature* **448**, 457–460 (2007).
21. G. Eda, M. Chhowalla, *Adv. Mater.* **22**, 2392–2415 (2010).
22. A. Lerf et al., *J. Phys. Chem. Solids* **67**, 1106–1110 (2006).
23. D. W. Boukhvalov, M. I. Katsnelson, Y.-W. Son, *Nano Lett.* **13**, 3930–3935 (2013).
24. S. You, S. M. Luzan, T. Szabó, A. V. Taluzin, *Carbon* **52**, 171–180 (2013).
25. Materials and methods are available as supplementary materials on Science Online.
26. B. Van der Bruggen, J. Schaep, D. Wilms, C. Vandecasteele, *J. Membr. Sci.* **156**, 29–41 (1999).
27. N. R. Wilson et al., *ACS Nano* **3**, 2547–2556 (2009).
28. D. Pacilé et al., *Carbon* **49**, 966–972 (2011).
29. N. Wei, Z. Xu, Breakdown of fast water transport in graphene oxides. arXiv:1308.5367.
30. S. Wang, H. Sun, H. M. Ang, M. O. Tade, *Chem. Eng. J.* **226**, 336–347 (2013).

Acknowledgments: This work was supported by the European Research Council, the Royal Society, Engineering and Physical Research Council (UK), and the National Natural Science Foundation (China). We thank A. Mishchenko and J. Waters for help. R.K.J. also acknowledges support by the Marie Curie Fellowship, and R.R.N. acknowledges support by the Leverhulme Trust and Bluestone Global Tech.

Supplementary Materials

www.sciencemag.org/content/343/6172/752/suppl/DC1
Materials and Methods

Figs. S1 to S4

Table S1

References (31–52)

9 September 2013; accepted 9 January 2014
10.1126/science.1245711

MATERIALS SCIENCE

Graphene Oxide Membranes for Ionic and Molecular Sieving

Baoxia Mi

Ionic and molecular sieving membranes that enable fast solute separations from aqueous solutions are essential for processes such as water purification and desalination, sensing, and energy production (1–3). The two-dimensional structure and tunable physicochemical properties of graphene oxide (GO) offer an exciting opportunity to make a fundamentally new class of sieving membranes by stacking GO nanosheets (4–6). In the layered GO membrane, water molecules permeate through the interconnected nanochannels formed between GO nanosheets and follow a tortuous path primarily over the hydrophobic nonoxidized surface rather than the hydrophilic oxidized region of GO (7). The nearly frictionless surface of the non-oxidized GO facilitates the extremely fast flow of water molecules (5). On page 752

of this issue, Joshi *et al.* (8) further report that ions smaller in size than the GO nanochannel can permeate in the GO membrane at a speed orders of magnitude faster than would occur through simple diffusion. Size exclusion appears to be the dominant sieving mechanism.

When dry, GO membranes made by vacuum filtration can be so tightly packed (with a void spacing of ~0.3 nm between GO nanosheets) that only water vapor aligned in a monolayer can permeate through the nanochannel (5). Joshi *et al.* found that when such a GO membrane was immersed in an ionic solution, hydration increased the GO spacing to ~0.9 nm (8). Any ion or molecule with a hydrated radius of 0.45 nm or less could enter the nanochannel, but all larger-sized species were blocked (see the figure).

Such a sharp size cutoff by the GO membrane has important implications in a myriad of separation applications. By adjusting the GO spacing through sandwiching appropriately sized spacers between GO nanosheets,

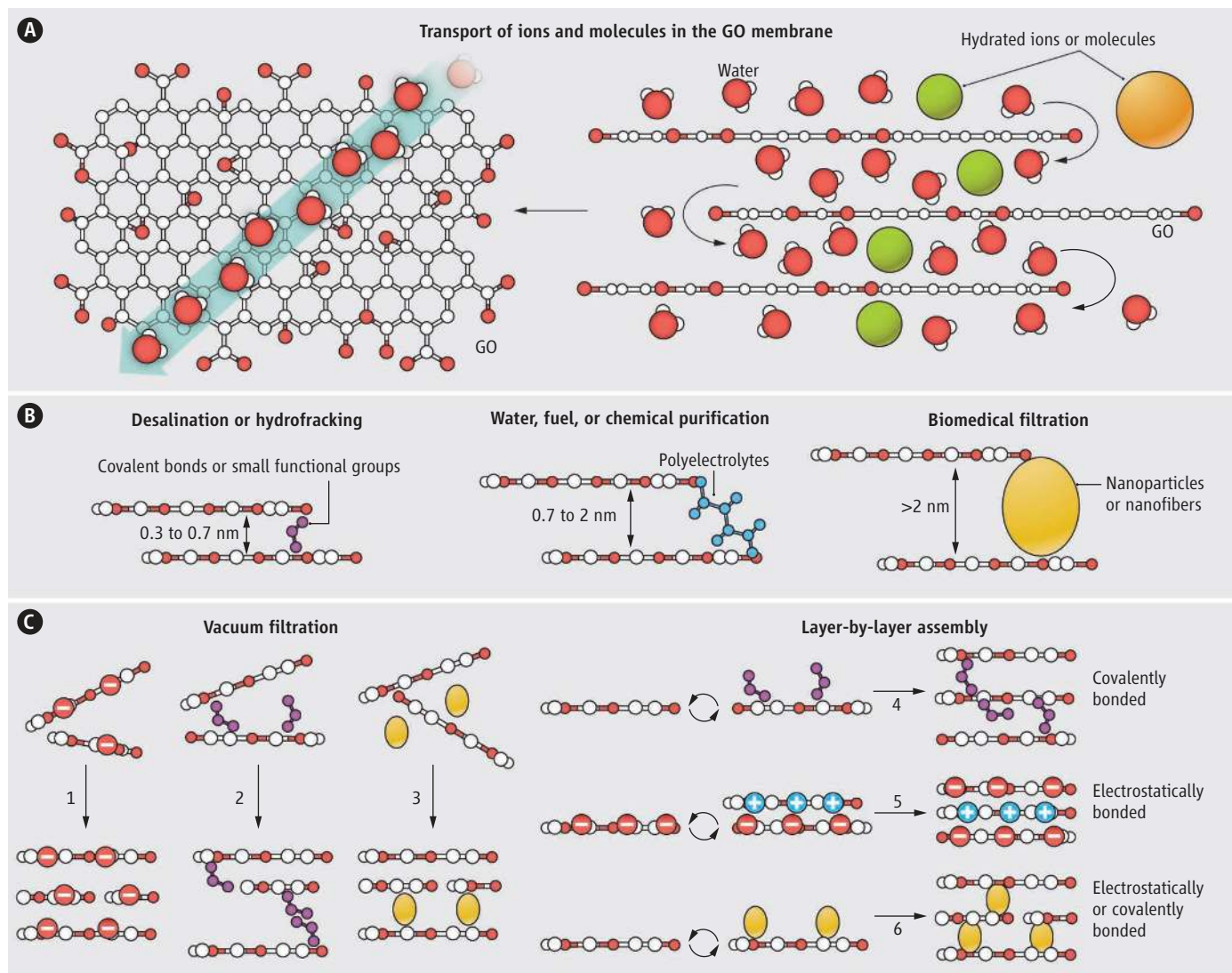
Membranes made by properly spacing and bonding stacked graphene oxide nanosheets enable precise, superfast sieving of ions and molecules.

a broad spectrum of GO membranes could be made, each being able to precisely separate target ions and molecules within a specific size range from bulk solution. Compared with the typically wide pore-size distribution of commonly used polymeric membranes, the narrow channel-size distribution of GO membranes is truly advantageous for precise sieving.

The hydration of GO in aqueous solution, however, makes it more challenging to manipulate the GO spacing within a subnanometer range than to enlarge it. For example, desalination requires that the GO spacing should be less than 0.7 nm to sieve the hydrated Na^+ (with a hydrated radius of 0.36 nm) from water. Such small spacing could be obtained by partially reducing GO to decrease the size of hydrated functional groups or by covalently bonding the stacked GO nanosheets with small-sized molecules to overcome the hydration force.

In contrast, an enlarged GO spacing (1 to 2 nm) can be conveniently achieved by

Department of Civil and Environmental Engineering, University of Maryland, 1161 Glenn L. Martin Hall, College Park, MD 20742, USA. E-mail: bmi@umd.edu



GO membranes. (A) Water and small-sized ions and molecules (compared with the void spacing between stacked GO nanosheets) permeate superfast in the GO membrane, but larger species are blocked. (B) The separation capability of the GO membrane is tunable by adjusting the nanochannel size. (C) Several meth-

ods for the synthesis of GO membranes have been reported or are envisioned; GO nanosheets can be physically packed by vacuum filtration (options 1 to 3), or they can be stabilized by covalent bonds, electrostatic forces, or both (options 4 to 6) during layer-by-layer assembly.

inserting large, rigid chemical groups (6) or soft polymer chains (e.g., polyelectrolytes) between GO nanosheets, resulting in GO membranes ideal for applications in water purification, wastewater reuse, and pharmaceutical and fuel separation. If even larger-sized nanoparticles or nanofibers are used as spacers, GO membranes with more than 2-nm spacing may be produced for possible use in biomedical applications (e.g., artificial kidneys and dialysis) that require precise separation of large biomolecules and small waste molecules.

GO membranes can be synthesized either by vacuum filtration or by layer-by-layer (LbL) assembly, both of which are conducted in aqueous solution without any organic solvent involved and, hence, are more environmentally friendly. The GO membranes

prepared by vacuum filtration, either from a pure GO solution or a mixture of GO and spacers, might lack sufficient bonding between GO nanosheets. Because of the high hydrophilicity of GO, these membranes are likely to disperse in water, especially under cross-flow conditions typically encountered in membrane operations. In contrast, the LbL method is ideal for introducing an interlayer stabilizing force via covalent bonding (6), electrostatic interaction, or both effects during layer deposition.

The GO membrane thickness can be readily controlled by varying the number of LbL deposition cycles. Theoretically, as few as two stacked GO layers would be needed to create a sieving channel. In reality, however, deposition of additional GO layers is warranted to counteract the detrimental

effects of possible defects and nonuniform deposition of GO nanosheets on the membrane's sieving capability. Finally, the LbL synthesis of GO membranes is highly scalable and cost-effective, unlike the challenging synthesis of monolayer graphene membranes, which requires the manufacturing of large-sized graphene sheets and the punching of nanopores with a narrow size distribution (9).

Indeed, the GO membrane represents a next generation of ultrathin, high-flux, and energy-efficient membranes for precise ionic and molecular sieving in aqueous solution, with applications in numerous important fields. Future research is needed to understand thoroughly the transport of water and solutes in the GO membrane, especially to fundamentally elucidate

other potential separation mechanisms (e.g., charge and adsorption effects) in addition to size exclusion. More research is also needed to address specific issues concerning various exciting yet challenging applications in desalination, hydrofracking water treatment, and energy production, as well as in biomedical and pharmaceutical fields. Other largely unexplored areas include making multifunc-

tional GO membranes with exceptional antifouling, adsorptive, antimicrobial, and photocatalytic properties.

References and Notes

1. M. A. Shannon *et al.*, *Nature* **452**, 301 (2008).
2. M. Elimelech, W. A. Phillip, *Science* **333**, 712 (2011).
3. D. L. Gin, R. D. Noble, *Science* **332**, 674 (2011).
4. L. Qiu *et al.*, *Chem. Commun. (Camb.)* **47**, 5810 (2011).
5. R. R. Nair, H. A. Wu, P. N. Jayaram, I. V. Grigorieva, A. K. Geim, *Science* **335**, 442 (2012).
6. M. Hu, B. Mi, *Environ. Sci. Technol.* **47**, 3715 (2013).
7. D. W. Boukhvalov, M. I. Katsnelson, Y. W. Son, *Nano Lett.* **13**, 3930 (2013).
8. R. K. Joshi *et al.*, *Science* **343**, 752 (2014).
9. E. N. Wang, R. Karnik, *Nat. Nanotechnol.* **7**, 552 (2012).

Acknowledgments: Supported by NSF Awards CBET 1154572 and 1158601.

10.1126/science.1250247



Supplementary Material for

Precise and Ultrafast Molecular Sieving through Graphene Oxide Membranes

R. K. Joshi, P. Carbone, F. C. Wang, V. G. Kravets, Y. Su, I. V. Grigorieva, H. A. Wu,
A. K. Geim,* R. R. Nair*

*Corresponding author. E-mail: rahul.raveendran-nair@manchester.ac.uk (R.R.N.); geim@man.ac.uk (A.K.G.)

Published 14 February 2014, *Science* **343**, 752 (2014)
DOI: 10.1126/science.1245711

This PDF file includes:

Materials and Methods

Figs. S1 to S4

Table S1

Full Reference List

Materials and Methods

1. Fabrication of GO membranes

Graphite oxide was prepared by exposing millimeter size flakes of natural graphite to concentrated sulfuric acid, sodium nitrate and potassium permanganate (Hummers' method) (31). Then, graphite oxide was exfoliated into monolayer flakes by sonication in water, which was followed by centrifugation at 10,000 rpm to remove remaining few-layer crystals. GO membranes were prepared by vacuum filtration of the resulting GO suspension through Anodisc alumina membranes that had straight pores with a diameter of 0.2 μm , length of 60 μm and porosity of $\approx 50\%$. By changing the volume of the filtered GO solution, we could control the thickness h of the resulting membranes, making them from 0.5 μm to more than 10 μm thick. For consistency, all the membranes described in this report were chosen to be 5 μm in thickness, unless a dependence on h was specifically investigated.

We normally left GO laminates on top of the Anodiscs because the latter added little to the permeation barrier but provided a valuable mechanical support for our membranes improving their stability. Nevertheless, we also checked influence of this porous support on the measured permeation and found the same properties for supported and free standing membranes (11).

Although graphite oxide is known to be soluble in water, the vacuum-filtered GO laminates were found to be highly stable in water, and it was practically impossible to re-disperse them without extensive sonication. No thinning of membranes was noticed in our filtration experiments lasting for many weeks. To quantify the solubility of GO laminates, we accurately measured their weight and thickness before and after immersing in water for two weeks. No weight or thickness loss could be detected within our accuracy of better than 1%.

2. Experimental setup

The permeation experiments were performed using a U-shaped device shown in Fig. 1B of the main text. It consisted of two tubular compartments fabricated either from glass or copper tubes (inner diameters of 25 mm), which were separated by the studied GO membranes. The membranes were glued to a Cu foil with an opening of 1 cm in diameter (see Fig. 1A of the main text). The copper foil was clamped between two O-rings, which provided a vacuum-tight seal between the two compartments. In a typical experiment, we filled one of the compartments (referred to as feed) with a salt or molecular solution up to a height of approximately 20 cm (0.1 L volume). The other (permeate) compartment was filled with deionized water to the same level. Note that the hydrostatic pressure due to level changes plays no role in our experiments where the permeation is driven by large concentration gradients. We used magnetic stirring in both feed and permeate compartments to avoid possible concentration gradients near the membranes (so-called concentration polarization effect).

The GO membranes including the entire assembly with the O-rings were thoroughly tested for any possible cracks and holes. In the first control experiment, GO membranes were substituted with a thin Cu film glued to the same Cu foil with all the other steps

remaining the same. Using a highly concentrated salt solution in the feed compartment, we could not detect any permeation. In the second experiment, we reduced GO membranes so that the interlayer separation decreased to $\approx 4 \text{ \AA}$ (11). No ionic permeation could be detected, which again proves the absence of pin holes in the original GO membrane. Finally and most conclusively, we used a helium-leak detector as described in ref. 11. No leak could be detected in our GO membranes both before and after permeation measurements.

We believe such extensive leak tests are very important for the following reasons. During the last two years, four groups (15-18) studied filtration properties of GO laminates and, although results varied widely due to different fabrication and measurement procedures, they reported appealing filtration characteristics including large water fluxes and notable rejection rates for certain salts. Unfortunately, large organic molecules were also found to pass through such GO filters (16-18). The latter observation is disappointing and would considerably limit interest in GO laminates as molecular sieves. However, this observation is also inconsistent with the known structure of GO laminates (20,21). Small ions can reasonably be expected to move between GO planes separated by $d \leq 13 \pm 1 \text{ \AA}$ (19,22) but large molecules that do not fit within the available interlayer space must not. In this respect, we note that the emphasis of the previous studies was on high water rates that were comparable to the rates used for industrial desalination. Accordingly, a high water pressure was applied (16-18) and the GO membranes were intentionally prepared as thin as possible, 10–50 nm thick (16,17). This thickness corresponds to only a few dozens of GO layers that are made of randomly stacked μm -sized crystallites rather than being continuous graphene sheets. We speculate that such thin stacks contained holes and cracks, through which large organic molecules could penetrate.

3. Monitoring ion diffusion by electrical measurements

For a quick qualitative test of ion permeation through GO membranes, we have used the setup shown in the inset of Fig. S1. The feed and permeate compartments were again separated by GO membranes. We used an assembly similar to that described above but instead of the Cu foil GO membranes were glued to a glass slide with a 2 mm aperture. In addition, the liquid cell was small and made entirely from Teflon to avoid electrical shorting. The feed compartment was initially filled with a few mL of a concentrated salt solution, and the permeate compartment contained a similar volume of deionized water. Our typical feed solution was approximately a million times more electrically conducting than deionized water at room temperature. Therefore, if ions diffuse through the membrane, this results in an increase in conductivity of water at the permeate side (15). Permeation of salts in concentrations at a sub- μM level can be detected in this manner. Resistance of the permeate was monitored by using a Keithley source meter and platinum wires as electrodes.

Figure S1 shows examples of our measurements for the case of NaCl and potassium ferricyanide $\text{K}_3[\text{Fe}(\text{CN})_6]$. The observed decrease of resistivity as a function of time demonstrates that NaCl permeates through the membrane. Similar behavior was observed for CuSO_4 , KCl and other tested salts with small ions (see the main text). On the other hand, no changes in conductivity of deionized water could be detected for a potassium ferricyanide solution during measurements lasting for many days (Fig. S1).

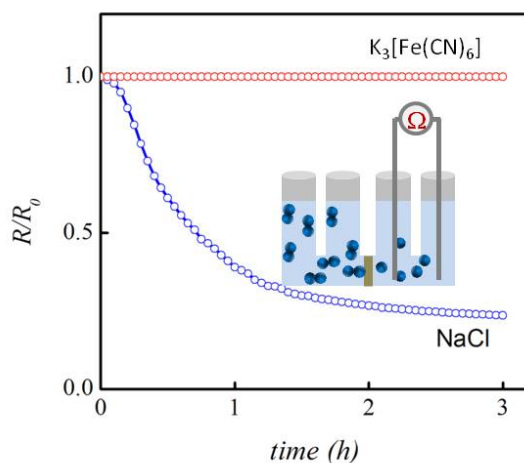


Fig. S1. Permeation of salts through GO membranes can be detected by using electrical measurements. The inset shows the measurement setup, and the main figure plots relative changes in resistivity of deionized water with time in the permeate compartment. Changes are normalized to an initial value of the measured resistance. Note that for the case of NaCl, the feed and permeate levels did not change with time, that is, no water flow was observed. This means that the primary permeation process was ion diffusion rather than osmosis, in contrast to the classic osmosis for the $K_3[Fe(CN)_6]$ case.

4. Quantitative analysis of ion and molecular permeation

The above electrical measurements show qualitatively that small ions can permeate through GO laminates whereas large ions such as $[Fe(CN)_6]^{3-}$ cannot. The technique is not applicable for molecular solutes because they exhibit little electrical conductivity. To gain quantitative information about the exact amount of permeating ions as well as to probe permeation of molecular solutes, we carried out chemical analysis of water at the permeate side. Samples were taken at regular intervals from a few hours to a few days and, in some cases, after several weeks. Due to different solubility of different solutes, we used different feed concentrations. They varied from 0.01 to 2 M, depending on a solute. For each salt, we performed measurements at several different feed concentrations to ensure that we worked in the linear response regime where the permeation rate was proportional to the feed concentration (Fig. 1C of the main text) and there was no sign of the concentration polarization effect.

The ion chromatography (IC) and the inductively coupled plasma optical emission spectrometry (ICP-OES) are the standard techniques used to analyze the presence of chemical species in solutions (32-34). We have employed the IC for anionic species, and the ICP-OES for cations. The measurement techniques provided us with values for ion concentrations in the permeate water. Using the known volume of the permeate (~ 0.1 L) we calculated the number of ions diffused into the permeate compartment. For certain salts (those with low solubility), the obtained permeate solutions were first concentrated by evaporation to improve the measurement accuracy. Furthermore, we crosschecked the results of our chemical analysis by weighing the dry material left after evaporation of water in the permeate compartment. This also allowed us to find the amount of salts

permeated through GO membranes. The weight and chemical analyses were in good quantitative agreement.

To detect organic solutes such as glycerol, sucrose and propanol, we employed the total organic carbon (TOC) analysis (34,35). No traces of glycerol and sucrose could be found in our permeate samples after several weeks, but propanol could permeate, although at a rate much lower than small ions as shown in Fig. 2 of the main text. The detection limit of our TOC was about 50 µg/L, and this put an upper limit on permeation of the solutes that could not be detected. The corresponding limiting values are shown by arrows in Fig. 2 of the main text. The above techniques were calibrated using several known concentrations of the studied solutes (typically, 4-5), and the detection limits were identified by decreasing the concentration of the standard solution until the measured signal became five times the baseline noise.

The optical absorption spectroscopy is widely used to detect solutes with absorption lines in the visible spectrum (1,12). We employed this technique for large ions such as $[\text{Fe}(\text{CN})_6]^{3-}$, $[\text{Ru}(\text{bipy})_3]^{2+}$ of Tris(bipyridine)ruthenium(II) dichloride ($[\text{Ru}(\text{bipy})_3]\text{Cl}_2$) and PTS^{4-} of pyrenetetrasulfonic acid tetrasodium salt (Na_4PTS). We could not detect any signatures of $[\text{Fe}(\text{CN})_6]^{3-}$, $[\text{Ru}(\text{bipy})_3]^{2+}$ and PTS^{4-} on the permeate side, even after many weeks of running the analysis. The absorption spectra were taken with an empty container as a background reference. The detection limit was estimated by measuring a reference solution and gradually decreasing its concentration by a factor of 2-3 until the optical absorption peaks completely disappeared. The penultimate concentration was chosen as the corresponding detection limits in Fig. 2 of the main text.

To calculate the ion permeation rates, J , expected for the network of capillaries present inside GO laminates, we have used the classical diffusion equation

$$J = D \times \Delta C \times A_{\text{eff}} / L_{\text{eff}}$$

where $D \approx 10^{-5} \text{ cm}^2/\text{s}$ is the diffusion coefficient for small ions in water and ΔC the concentration gradient across the membrane ($\Delta C \approx 23 \text{ g/L}$ if a 1M solution of a Na salt is taken as an example). For a 5 micron thick GO membrane with an area of 1 cm^2 , the effective area A_{eff} of the water column through which the diffusion can occur is given by $A_{\text{eff}} \approx 1 \text{ cm}^2 \times d/L \approx 10^{-3} \text{ cm}^2$. The effective length of this column is $L_{\text{eff}} \approx L \times h/d \approx 0.5 \text{ cm}$. Putting the numbers into the above equation, we find $J \approx 0.5 \text{ ng/s}$ or $\approx 2 \times 10^{-3} \text{ mg/h}$ per square cm or $\approx 10^{-3} \text{ mol/h/m}^2$. As discussed in the main text and ref. 11, the estimated space available for ion diffusion has been verified by other experiments and is likely to be an overestimate. Despite this, J is still $\approx 3,000$ times smaller than the measured rate in Fig. 2. In fact, the observed ion permeability of our GO membranes is as large as the one we measured for a sheet of the standard filter paper.

Note that the ultrafast salt permeation does not contradict to the 20 to 60% rejection rates reported in refs 16 and 17. The rejection rates were measured with respect to a water flow driven by a large hydrostatic pressure. In this case, both salt and water move through the GO laminate with little impedance. Note that 50% rejection means the relative number of ions with respect to the number of water molecules is reduced only by a factor of 2 after the filtration. Furthermore, in our experiments with small salts, we did not observe any noticeable change in water levels, which indicates little osmotic pressure. Therefore, ions diffuse through a nearly static column of water inside GO capillaries.

5. Tested solutes and their hydrated radii

Figure 2 of the main text summarizes the results of our experiments by plotting the observed permeation rates as a function of the hydrated radius for all the solutes that have been analyzed quantitatively in our work. Values of the hydrated radius for eleven of them can be found in the literature (13,26,36,37) and are shown in Table S1. To the best of our knowledge, there exist no literature values for propanol, sucrose, glycerol and PTS⁴⁻. In the latter case, we have estimated their hydrated radii by using Stokes/crystal radii (26,38). To this end, we have plotted the known hydrated radii as a function of the known Stokes radii, which yields a simple linear dependence. Hydrated radii for the remaining 4 species can then be estimated by using this dependence and their known Stokes radii. The resulting hydrated radii are added to Table S1.

Ion/molecule	Hydrated radius (Å)
K ⁺	3.31
Cl ⁻	3.32
Na ⁺	3.58
CH ₃ COO ⁻	3.75
SO ₄ ²⁻	3.79
AsO ₄ ³⁻	3.85
CO ₃ ²⁻	3.94
Cu ²⁺	4.19
Mg ²⁺	4.28
propanol	4.48
glycerol	4.65
[Fe(CN) ₆] ³⁻	4.75
sucrose	5.01
(PTS) ⁴⁻	5.04
[Ru(bipy) ₃] ²⁺	5.90

Table S1. List of analyzed species and their hydrated radii.

In principle, one can also consider using the Stokes rather than hydrated radius as a running parameter in Fig. 2 of the main text. In this case, the general trend of blocking large molecules and allowing small ones remains the same. However, the functional form in Fig. 2 would be no longer single-valued near the cutoff, which is why we have chosen heuristically (and for the physics reasons as well) to use the hydrated radius.

6. Salt absorption by graphene laminates

To test the absorbing efficiency of GO laminates with respect to salts, we have carried out the following experiments. Our GO membranes were accurately weighed and

placed in a salt solution with concentration C (we used MgCl_2 , KCl and $\text{K}_3[\text{Fe}(\text{CN})_6]$). After several hours, the laminates were taken out, rinsed with deionized water and dried. An intake of the salts was measured at a relative humidity of $50 \pm 10\%$, same as the initial weight measurements. Figure S2A shows that for the salt that cannot permeate through GO laminates, there was no increase in weight. On the other hand, for small salts that fit inside GO capillaries, we observed a massive intake that reached up to 25% in weight. The intake rapidly saturated at relatively small C of ≈ 0.1 M (see Fig. S2A).

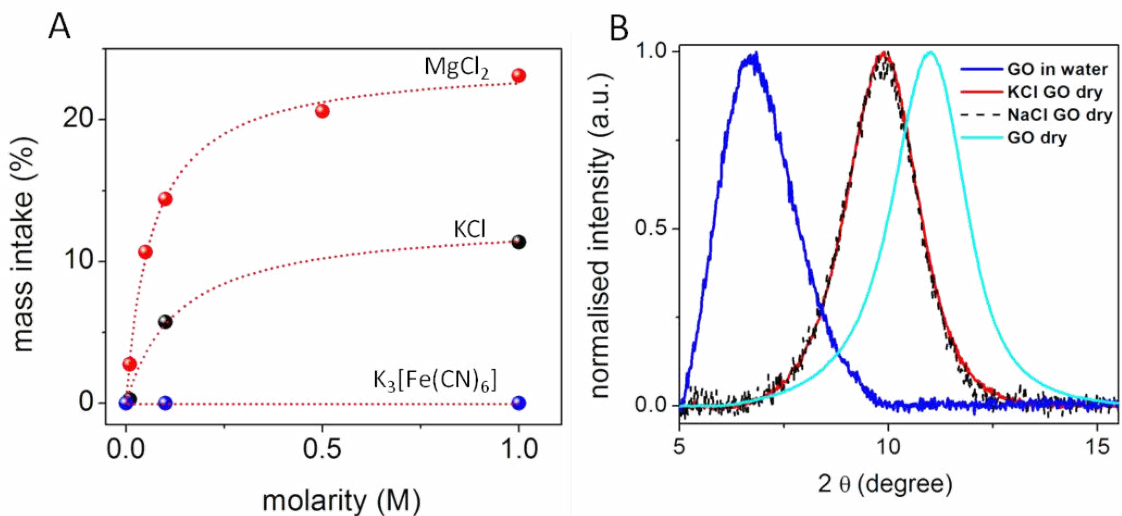


Fig. S2. Salt intake by GO laminates. **(A)** Relative increase in weight for $5\mu\text{m}$ thick laminates soaked in different solutions. No intake could be detected for $\text{K}_3[\text{Fe}(\text{CN})_6]$ but it was large for small-radius salts. The dotted curves represent the best fit by the Langmuir isotherm. **(B)** X-ray diffraction for pristine GO, GO soaked in NaCl and GO soaked in KCl . All these measurements were carried out at a relative humidity of $50 \pm 10\%$. The blue curve shows the interlayer diffraction peak for GO immersed in water.

The mass intake in Figure S2A can be due to either dry salts or extra water accumulated inside the capillaries in the presence of the salts. We were able to separate the contributions by using the following complementary approaches. In the first one, a GO laminate was dried in zero humidity of a glove box for one week and accurately weighted. Then, the laminate sample was exposed to a 1M MgCl_2 solution and dried again in zero humidity for a week. We found a mass intake of $13 \pm 2\%$, that is, notably smaller than that in Fig. S2A. The same result was confirmed by the second approach using chemical analysis. A sample of the same GO laminate exposed to a 1M MgCl_2 solution was dissolved in a mixture of nitric, sulphuric and perchloric acids at 300°C , which effectively turned carbon into CO_2 (chemical burning of graphene). After this, ICP-OES (using iCap 6300) was employed to measure the amount of Mg in the resulting solution. We found 3-3.2% of Mg in weight, which translates into $\approx 13\%$ mass intake of MgCl_2 from a 1M solution, in agreement with the above result based on weighing. This percentage means that more than a half of the intake in Fig. S2A was due to the dry salt with the rest being additional bound water.

The large salt intake proves that the permeating solutes accumulate inside GO capillaries, leading to highly concentrated solutions internally. Using the measured amount of absorbed salts and the known amount of water in fully hydrated GO laminates (see below), we estimate that internal concentrations can reach several molar, that is, can exceed external C by a factor of 10 or more. This highly-efficient absorption of small salts by GO laminates is in agreement with the absorbing properties reported previously for graphene and graphite-oxide powders (30) and sheds light on the mechanism behind those observations.

The accumulation of salts inside GO capillaries implies that there is an energy gain when ions move inside graphene capillaries from the bulk solution (39). Our MD simulations (below) confirm this effect and indicate that the energy gain is mostly due to interaction of ions with graphene walls. The ionic absorption is reminiscent of the standard capillary effect where water molecules gain energy by moving inside hydrophilic tubes. In our case, water plays a role of a continuous medium in which the capillary-like pressure acts on ions, sucking them inside capillaries from the bulk water.

7. X-ray analysis of GO laminates

We have also investigated our GO laminates by using X-ray diffraction. Figure S2B shows the diffraction peak for GO at a relative humidity of $\approx 50\%$. It corresponds to the interlayer separation $d \approx 8 \text{ \AA}$. For GO laminates immersed in water, the peak is shifted to $d \approx 13 \text{ \AA}$, in agreement with literature values (19,22). It is interesting to note that the peak in water has not become notably broader. This means that the layered structure of GO laminates is preserved in the fully immersed state, that is, the additional water is adsorbed as an extra layer with a rather uniform thickness of $\approx 5 \text{ \AA}$. Taking into account that d for reduced GO is $\approx 4 \text{ \AA}$, there is a free space of $9 \pm 1 \text{ \AA}$ between graphene sheets, which is available for transport of water. The latter value is in agreement with the permeation cutoff observed both experimentally and in our MD simulations.

We have also measured the volume of taken-in water by weighing. GO laminates exposed to nearly 100% humidity exhibited a water intake that was equal to approximately $h \times S$ where S is the laminate area and h its thickness. This is the volume of graphene capillaries, which is used to estimate diffusion through the equivalent water column (see the main text). The found capillary volume is also consistent with alternative estimates reported in ref. 11.

When our GO laminates were soaked in NaCl or KCl solutions and then dried out at the same $50 \pm 10\%$ humidity as above, d increased from 8 to 9 \AA (see Fig. S2B). This increase in the interlayer spacing is consistent with the fact that a significant amount of salts is trapped within graphene capillaries. On the other hand, d for GO inside a concentrated salt solution was found similar to that for GO in clean water ($13 \pm 1 \text{ \AA}$). The latter observation is attributed to the fact that d is determined by the number of intercalating atomic layers of water and ions move inside this water layer, in agreement with our MD simulations.

8. Molecular dynamics simulations

Our basic modeling setup consisted of two equal water reservoirs connected by a capillary formed by parallel graphene sheets as shown in Fig. 3A of the main text. Sizes

of the reservoirs and capillaries varied in different modeling experiments. To analyze the absorption of salts and study ion diffusion in the confined geometry, we used reservoirs with a height of 51.2 Å, a length of 50 Å and a depth of 49.2 Å, which were connected by a 30 Å long capillary. A slightly smaller setup was used to assess sieving properties of graphene capillaries. It consisted of the reservoirs with a height of 23.6 Å, a length of 50 Å and a depth of 30.1 Å, which were connected by a 20 Å long capillary. For both setups, we varied the capillary width d from 7 to 13 Å (d is the distance between the centers of the graphene sheets). When the same property was modeled, both setups yielded similar behavior.

Periodic boundary conditions were applied in the Z direction, that is, along the capillary depth. Ions or molecules were added until the desired molar concentrations were reached. Water was modeled by using the simple point charge model (40,41). Sodium and chlorine ions were modeled by using the parameters from refs 42-43; magnesium and copper anions with the OPLS-AA parameters (44). Intermolecular interactions were described by the 12-6 Lennard-Jones (LJ) potential together with a Coulomb potential. Parameters for water-graphene interactions were reported in refs 45-46.

The system was initially equilibrated at 300 K with a coupling time of 0.1 ps⁻¹ for 500 ps (47). In the modeling of sieving properties, our typical simulation runs were 100 ns long and obtained in the isobaric ensemble at the atmospheric pressure where the simulation box was allowed to change only in the X and Y direction with a pressure coupling time of 1 ps⁻¹ (45) and a compressibility of 4.5×10⁻⁵ bar⁻¹. The cutoff distance for nonbonding interactions was set up at 10 Å, and the particle mesh Ewald summations method was used to model the system's electrostatics (48). During simulations, all the graphene atoms were held in fixed positions whereas other bonds were treated as flexible. A time step of 1 fs was employed.

To model sieving properties of graphene, the GROMACS software was used (49). At the beginning of each simulation run, water molecules rapidly filled the graphene capillary forming one, two or three layer structures, depending on d , in agreement with the previous reports (11,29). Then after a certain period of time, which depended on a solute in the feed reservoir, ions/molecules started enter the capillary and eventually reached the pure water reservoir for all the modeled solutes, except for toluene and octanol. The found permeation rates are shown in Fig. 3B of the main text. We have also noticed that cations and anions move through the capillary together and without noticeably changing their hydration shells.

9. Theoretical analysis of permeation for large molecules

In the case of organic molecules (for example, propanol) our simulations showed that the molecules entered the graphene capillary but then rapidly formed clusters that resided inside the capillary for a long time. The cluster formation is probably due to confinement. On the other hand, the long residence times can be attributed to van der Waals forces between the alcohol molecules and graphene (50). Toluene molecules exhibited even stronger interaction with graphene (due to π - π staking). In our simulations, toluene molecules entered the channel but never left it being adsorbed to graphene walls (Fig. S3). This adsorption is likely to be responsible for the experimentally undetectable level of toluene permeation. Therefore, despite our experimental data exhibit a rather simple sieving behavior that can be explained just by

the physical size effect, we believe that van der Waals interactions between solutes and graphene may also play a role in limiting permeation for those molecules and ions that have sizes close to the cutoff radius.

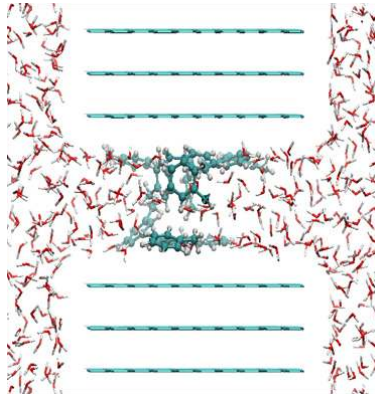


Fig. S3. Snapshot of our MD simulations for toluene in water. All toluene molecules are trapped inside the short graphene channel and none leaves it even after 100 ns.

To better understand the observed sieving effect with its sharp mechanical cutoff, we performed the following analysis. An artificial cluster was modeled as a truncated icosahedron and placed in the middle of the capillary as shown in the inset of Fig. 3B of the main text. The size of the cluster was varied by changing the distance between the constituent 60 atoms, and the interaction energy between the cluster and the graphene capillary was calculated. The energy was computed as the sum of interactions between all the atoms involved which were modeled with a 12-6 LJ potential. Positive and negative values of the calculated energy indicate whether the presence of the cluster in the capillary is energetically favorable or not, respectively. The minimum radius for which the spherical cluster was allowed into the graphene capillary obviously depended on the capillary size. For capillaries that allowed two layers of waters ($d = 9 \text{ \AA}$) this radius was found to be 4.7 \AA . For capillaries containing three water layers ($d = 13 \text{ \AA}$), the radius was 5.8 \AA . These values are shown in Fig. 3B of the main text as the blue bars.

10. Simulations of salt absorption

In this case, we employed a relatively long capillary (482 \AA) such that its volume was comparable to that of the reservoirs (see Fig. S4A). The capillary width was varied between 9 and 11 \AA , which corresponds to 2 and 3 atomic layers of water. MD simulations were carried out in a canonical ensemble using LAMMPS (51). The temperature was set at 300 K by using the Nose-Hoover thermostat. The equations of motion were integrated using a velocity-Verlet scheme with a time step of 1.0 fs . The snapshots obtained in these simulations (for example, see Fig. S4A) were processed by *Atomeye* (52).

During the simulations, we counted the number of ions inside the capillary as a function of time (Fig. S4B). If the initial concentration C of NaCl was taken constant over the entire system (for example, $C = 1 \text{ M}$ for the black curve in Fig. S4B), we found that the salt moved from the reservoirs into the capillary, that is, ions were attracted to the confined region. Then, we used smaller initial C inside the two reservoirs (0.1 and 0.5 M)

while keeping the same $C = 1$ M inside the capillary. Despite the large concentration gradient, the salt still moved into the capillary rather than exited it (see Fig. S4B).

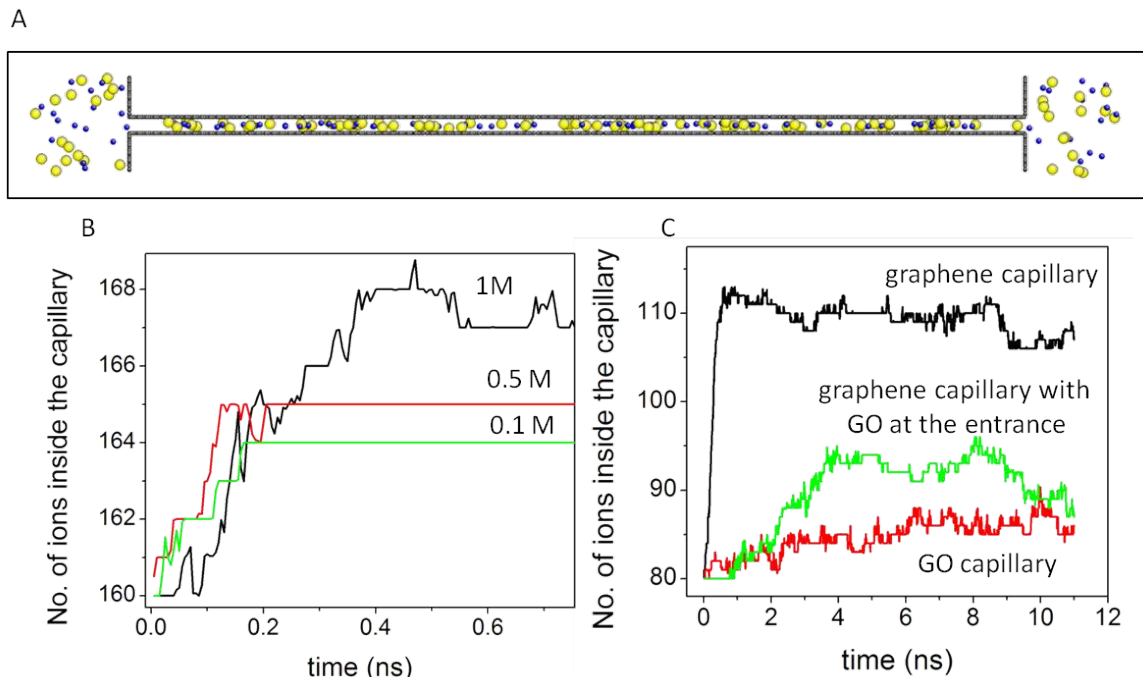


Fig. S4. Simulated salt-absorption effect. (A) Snapshot for the case of a 1M NaCl solution inside the capillary and 0.1 M in the reservoirs (water molecules are removed for clarity). Despite the large concentration gradient, ions move from the reservoirs into the capillary. (B) Number of ions inside a 9 Å wide capillary (two layers of water) as a function of simulation time. Initial concentrations of NaCl in the two reservoirs are 0.1, 0.5 and 1 M for the different curves. The initial NaCl concentration inside the capillary is 1 M for all the curves. (C) Comparison between graphene and GO capillaries. Evolution of the number of ions inside a capillary (11 Å wide) for initial $C = 1$ M throughout the system.

In the next MD simulation experiment, we kept a low concentration of NaCl in the two reservoirs ($C = 0.1$ M) and gradually increased C inside the graphene capillary up to 3 M. For $C = 2$ M inside it, we still observed an influx of NaCl from the reservoirs. The salt started leaving the capillary only if C inside approached ~ 3 M. This allows an estimate of the equilibrium concentration of NaCl inside the graphene capillary as close to 3 M, in agreement with the experimental results discussed in section #6. The concentration gradient corresponds to a capillary-like pressure of >50 bars, which acts on salt ions against the concentration gradient. To find an average speed of ionic flow caused by this pressure, further work is required, especially because the viscosity experienced by ion moving against graphene walls is likely to be different from that for water molecules (11).

We have also assessed the possibility that functionalized GO regions can play a notable role in salt absorption and, more generally, in molecular permeation through GO laminates. To this end, we used the same MD setups as described above but added

hydroxyl and epoxy groups to both walls of graphene capillaries. The epoxy group was modeled by binding an oxygen atom to two carbon atoms of graphene and the hydroxyl group (OH) by its oxygen bonded to a carbon atom. For simplicity, oxygen atoms were fixed in their positions whereas the O-H bond was treated as flexible. Figure S4C shows an example of the latter simulations. Both ion and water dynamics inside GO capillaries were found to be extremely slow, in agreement with the assumptions of our previous work (11) and a recent MD report by another group (29). In addition, we considered the case where only entrances of the graphene capillary were covered with hydroxyl and epoxy groups (Fig. S4C). These simulations again showed slow dynamics, similar to the case of fully-covered GO capillaries. Accordingly, we expect that in our observations functionalized regions play a lesser role than pristine capillaries.

References and Notes

1. K. B. Jirage, J. C. Hulteen, C. R. Martin, Nanotubule-based molecular-filtration membranes. *Science* **278**, 655–658 (1997). [doi:10.1126/science.278.5338.655](https://doi.org/10.1126/science.278.5338.655)
2. N. B. McKeown, P. M. Budd, Polymers of intrinsic microporosity (PIMs): Organic materials for membrane separations, heterogeneous catalysis and hydrogen storage. *Chem. Soc. Rev.* **35**, 675–683 (2006). [doi:10.1039/b600349d](https://doi.org/10.1039/b600349d) [Medline](#)
3. D. L. Gin, R. D. Noble, Chemistry. Designing the next generation of chemical separation membranes. *Science* **332**, 674–676 (2011). [doi:10.1126/science.1203771](https://doi.org/10.1126/science.1203771)
4. D. Cohen-Tanugi, J. C. Grossman, Water desalination across nanoporous graphene. *Nano Lett.* **12**, 3602–3608 (2012). [doi:10.1021/nl3012853](https://doi.org/10.1021/nl3012853) [Medline](#)
5. S. P. Koenig, L. Wang, J. Pellegrino, J. S. Bunch, Selective molecular sieving through porous graphene. *Nat. Nanotechnol.* **7**, 728–732 (2012). [doi:10.1038/nnano.2012.162](https://doi.org/10.1038/nnano.2012.162) [Medline](#)
6. M. Ulbricht, Advanced functional polymer membranes. *Polymer (Guildf.)* **47**, 2217–2262 (2006). [doi:10.1016/j.polymer.2006.01.084](https://doi.org/10.1016/j.polymer.2006.01.084)
7. M. Elimelech, W. A. Phillip, The future of seawater desalination: Energy, technology, and the environment. *Science* **333**, 712–717 (2011). [doi:10.1126/science.1200488](https://doi.org/10.1126/science.1200488)
8. J. K. Holt, H. G. Park, Y. Wang, M. Stadermann, A. B. Artyukhin, C. P. Grigoropoulos, A. Noy, O. Bakajin, Fast mass transport through sub-2-nanometer carbon nanotubes. *Science* **312**, 1034–1037 (2006). [doi:10.1126/science.1126298](https://doi.org/10.1126/science.1126298)
9. M. Majumder, N. Chopra, R. Andrews, B. J. Hinds, Nanoscale hydrodynamics: Enhanced flow in carbon nanotubes. *Nature* **438**, 44 (2005). [doi:10.1038/438044a](https://doi.org/10.1038/438044a) [Medline](#)
10. G. Hummer, J. C. Rasaiah, J. P. Noworyta, Water conduction through the hydrophobic channel of a carbon nanotube. *Nature* **414**, 188–190 (2001). [doi:10.1038/35102535](https://doi.org/10.1038/35102535) [Medline](#)
11. R. R. Nair, H. A. Wu, P. N. Jayaram, I. V. Grigorieva, A. K. Geim, Unimpeded permeation of water through helium-leak-tight graphene-based membranes. *Science* **335**, 442–444 (2012). [doi:10.1126/science.1211694](https://doi.org/10.1126/science.1211694)
12. M. Majumder, N. Chopra, B. J. Hinds, Effect of tip functionalization on transport through vertically oriented carbon nanotube membranes. *J. Am. Chem. Soc.* **127**, 9062–9070 (2005). [doi:10.1021/ja043013b](https://doi.org/10.1021/ja043013b) [Medline](#)
13. F. Fornasiero, H. G. Park, J. K. Holt, M. Stadermann, C. P. Grigoropoulos, A. Noy, O. Bakajin, Ion exclusion by sub-2-nm carbon nanotube pores. *Proc. Natl. Acad. Sci. U.S.A.* **105**, 17250–17255 (2008). [doi:10.1073/pnas.0710437105](https://doi.org/10.1073/pnas.0710437105) [Medline](#)
14. L. Qiu, X. Zhang, W. Yang, Y. Wang, G. P. Simon, D. Li, Controllable corrugation of chemically converted graphene sheets in water and potential application for nanofiltration. *Chem. Commun. (Camb.)* **47**, 5810–5812 (2011). [doi:10.1039/c1cc10720h](https://doi.org/10.1039/c1cc10720h) [Medline](#)
15. P. Sun, M. Zhu, K. Wang, M. Zhong, J. Wei, D. Wu, Z. Xu, H. Zhu, Selective ion penetration of graphene oxide membranes. *ACS Nano* **7**, 428–437 (2013). [doi:10.1021/nn304471w](https://doi.org/10.1021/nn304471w) [Medline](#)

16. Y. Han, Z. Xu, C. Gao, Ultrathin graphene nanofiltration membrane for water purification. *Adv. Funct. Mater.* **23**, 3693–3700 (2013). [doi:10.1002/adfm.201202601](https://doi.org/10.1002/adfm.201202601)
17. M. Hu, B. Mi, Enabling graphene oxide nanosheets as water separation membranes. *Environ. Sci. Technol.* **47**, 3715–3723 (2013). [doi:10.1021/es400571g](https://doi.org/10.1021/es400571g) [Medline](#)
18. H. Huang, Y. Mao, Y. Ying, Y. Liu, L. Sun, X. Peng, Salt concentration, pH and pressure controlled separation of small molecules through lamellar graphene oxide membranes. *Chem. Commun. (Camb.)* **49**, 5963–5965 (2013). [doi:10.1039/c3cc41953c](https://doi.org/10.1039/c3cc41953c) [Medline](#)
19. K. Raidongia, J. Huang, Nanofluidic ion transport through reconstructed layered materials. *J. Am. Chem. Soc.* **134**, 16528–16531 (2012). [doi:10.1021/ja308167f](https://doi.org/10.1021/ja308167f) [Medline](#)
20. D. A. Dikin, S. Stankovich, E. J. Zimney, R. D. Piner, G. H. Dommett, G. Evmenenko, S. T. Nguyen, R. S. Ruoff, Preparation and characterization of graphene oxide paper. *Nature* **448**, 457–460 (2007). [doi:10.1038/nature06016](https://doi.org/10.1038/nature06016) [Medline](#)
21. G. Eda, M. Chhowalla, Chemically derived graphene oxide: towards large-area thin-film electronics and optoelectronics. *Adv. Mater.* **22**, 2392–2415 (2010). [doi:10.1002/adma.200903689](https://doi.org/10.1002/adma.200903689) [Medline](#)
22. A. Lerf, A. Buchsteiner, J. Pieper, S. Schöttl, I. Dekany, T. Szabo, H. P. Boehm, Hydration behavior and dynamics of water molecules in graphite oxide. *J. Phys. Chem. Solids* **67**, 1106–1110 (2006). [doi:10.1016/j.jpcs.2006.01.031](https://doi.org/10.1016/j.jpcs.2006.01.031)
23. D. W. Boukhvalov, M. I. Katsnelson, Y.-W. Son, Origin of anomalous water permeation through graphene oxide membrane. *Nano Lett.* **13**, 3930–3935 (2013). [doi:10.1021/nl4020292](https://doi.org/10.1021/nl4020292) [Medline](#)
24. S. You, S. M. Luzan, T. Szabó, A. V. Taluzin, A. V. Effect of synthesis method on solvation and exfoliation of graphite oxide. *Carbon* **52**, 171–180 (2013). [doi:10.1016/j.carbon.2012.09.018](https://doi.org/10.1016/j.carbon.2012.09.018)
25. Materials and methods are available as supplementary materials on *Science Online*.
26. B. Van der Bruggen, J. Schaep, D. Wilms, C. Vandecasteele, Influence of molecular size, polarity and charge on the retention of organic molecules by nanofiltration. *J. Membr. Sci.* **156**, 29–41 (1999). [doi:10.1016/S0376-7388\(98\)00326-3](https://doi.org/10.1016/S0376-7388(98)00326-3)
27. N. R. Wilson, P. A. Pandey, R. Beanland, R. J. Young, I. A. Kinloch, L. Gong, Z. Liu, K. Suenaga, J. P. Rourke, S. J. York, J. Sloan, Graphene oxide: Structural analysis and application as a highly transparent support for electron microscopy. *ACS Nano* **3**, 2547–2556 (2009). [doi:10.1021/nn900694t](https://doi.org/10.1021/nn900694t) [Medline](#)
28. D. Pacilé, J. C. Meyer, A. Fraile Rodríguez, M. Papagno, C. Gómez-Navarro, R. S. Sundaram, M. Burghard, K. Kern, C. Carbone, U. Kaiser, Electronic properties and atomic structure of graphene oxide membranes. *Carbon* **49**, 966–972 (2011). [doi:10.1016/j.carbon.2010.09.063](https://doi.org/10.1016/j.carbon.2010.09.063)
29. N. Wei, Z. Xu, Breakdown of fast water transport in graphene oxides. arXiv:1308.5367.
30. S. Wang, H. Sun, H. M. Ang, M. O. Tade, Adsorptive remediation of environmental pollutants using novel graphene-based nanomaterials. *Chem. Eng. J.* **226**, 336–347 (2013). [doi:10.1016/j.cej.2013.04.070](https://doi.org/10.1016/j.cej.2013.04.070)

31. W. S. Hummers, Jr., R. E. Offeman, Preparation of graphitic oxide. *J. Am. Chem. Soc.* **80**, 1339 (1958). [doi:10.1021/ja01539a017](https://doi.org/10.1021/ja01539a017)
32. P. E. Jackson, *Ion Chromatography in Environmental Analysis. Encyclopedia of Analytical Chemistry* (Wiley, New York, 2006).
33. J. Yeo, S. Y. Kim, S. Kim, D. Y. Ryu, T. H. Kim, M. J. Park, Mechanically and structurally robust sulfonated block copolymer membranes for water purification applications. *Nanotechnology* **23**, 245703 (2012). [doi:10.1088/0957-4484/23/24/245703](https://doi.org/10.1088/0957-4484/23/24/245703) [Medline](#)
34. N. T. Hancock, P. Xu, M. J. Roby, J. D. Gomez, T. Y. Cath, Towards direct potable reuse with forward osmosis: Technical assessment of long-term process performance at the pilot scale. *J. Membr. Sci.* **445**, 34–46 (2013). [doi:10.1016/j.memsci.2013.04.056](https://doi.org/10.1016/j.memsci.2013.04.056)
35. N. Ma, Y. Zhang, X. Quan, X. Fan, H. Zhao, Performing a microfiltration integrated with photocatalysis using an Ag-TiO₂/HAP/Al₂O₃ composite membrane for water treatment: Evaluating effectiveness for humic acid removal and anti-fouling properties. *Water Res.* **44**, 6104–6114 (2010). [doi:10.1016/j.watres.2010.06.068](https://doi.org/10.1016/j.watres.2010.06.068) [Medline](#)
36. E. R. Nightingale Jr., Phenomenological theory of ion solvation. Effective radii of hydrated Ions. *J. Phys. Chem.* **63**, 1381–1387 (1959). [doi:10.1021/j150579a011](https://doi.org/10.1021/j150579a011)
37. S. G. Schultz, A. K. Solomon, Determination of the effective hydrodynamic radii of small molecules by viscometry. *J. Gen. Physiol.* **44**, 1189–1199 (1961). [doi:10.1085/jgp.44.6.1189](https://doi.org/10.1085/jgp.44.6.1189) [Medline](#)
38. D. S. Tawfik, R. E. Viola, Arsenate replacing phosphate: Alternative life chemistries and ion promiscuity. *Biochemistry* **50**, 1128–1134 (2011). [doi:10.1021/bi200002a](https://doi.org/10.1021/bi200002a) [Medline](#)
39. G. Shi, Y. Ding, H. Fang, Unexpectedly strong anion- π interactions on the graphene flakes. *J. Comput. Chem.* **33**, 1328–1337 (2012). [doi:10.1002/jcc.22964](https://doi.org/10.1002/jcc.22964) [Medline](#)
40. H. J. C. Berendsen, J. P. M. Postma, W. F. van Gunsteren, J. Hermans, in *Intermolecular Forces* (Springer, Netherlands, 1981) vol. 14, pp. 331–342.
41. H. J. C. Berendsen, J. R. Grigera, T. P. Straatsma, The missing term in effective pair potentials. *J. Phys. Chem.* **91**, 6269–6271 (1987). [doi:10.1021/j100308a038](https://doi.org/10.1021/j100308a038)
42. D. E. Smith, X. D. Liem, Computer simulations of NaCl association in polarizable water. *J. Chem. Phys.* **100**, 3757–3766 (1994). [doi:10.1063/1.466363](https://doi.org/10.1063/1.466363)
43. S. Chowdhuri, A. Chandra, Molecular dynamics simulations of aqueous NaCl and KCl solutions: Effects of ion concentration on the single-particle, pair, and collective dynamical properties of ions and water molecules. *J. Chem. Phys.* **115**, 3732–3741 (2001). [doi:10.1063/1.1387447](https://doi.org/10.1063/1.1387447)
44. W. L. Jorgensen, D. S. Maxwell, J. Tirado-Rives, Development and testing of the OPLS all-atom force field on conformational energetics and properties of organic liquids. *J. Am. Chem. Soc.* **118**, 11225–11236 (1996). [doi:10.1021/ja9621760](https://doi.org/10.1021/ja9621760)
45. A. Cheng, W. A. Steele, Computer simulation of ammonia on graphite. I. Low temperature structure of monolayer and bilayer films. *J. Chem. Phys.* **92**, 3858–3866 (1990). [doi:10.1063/1.458562](https://doi.org/10.1063/1.458562)

46. T. Werder, J. H. Walther, R. L. Jaffe, T. Halicioglu, P. Koumoutsakos, On the water-carbon interaction for use in molecular dynamics simulations of graphite and carbon nanotubes. *J. Phys. Chem. B* **107**, 1345–1352 (2003). [doi:10.1021/jp0268112](https://doi.org/10.1021/jp0268112)
47. H. J. C. Berendsen, J. P. M. Postma, W. F. V. Gunsteren, A. DiNola, J. R. Haak, Molecular dynamics with coupling to an external bath. *J. Chem. Phys.* **81**, 3684–3690 (1984). [doi:10.1063/1.448118](https://doi.org/10.1063/1.448118)
48. E. Ulrich *et al.*, A smooth particle mesh Ewald method. *J. Chem. Phys.* **103**, 8577–8593 (1995). [doi:10.1063/1.470117](https://doi.org/10.1063/1.470117)
49. E. L. D. van der Spoel *et al.*, *Gromacs User Manual*, version 4.5 (2011).
50. T. Marosi, I. Dékány, G. Lagaly, Displacement processes on hydrophilic/hydrophobic surfaces in 1-propanol-water mixtures. *Colloid Polym. Sci.* **272**, 1136–1142 (1994). [doi:10.1007/BF00652383](https://doi.org/10.1007/BF00652383)
51. S. J. Plimpton, Fast parallel algorithms for short-range molecular dynamics. *J. Comput. Phys.* **117**, 1–19 (1995). [doi:10.1006/jcph.1995.1039](https://doi.org/10.1006/jcph.1995.1039)
52. J. Li, AtomEye: An efficient atomistic configuration viewer. *Model. Simul. Mater. Sci. Eng.* **11**, 173–177 (2003). [doi:10.1088/0965-0393/11/2/305](https://doi.org/10.1088/0965-0393/11/2/305)